

## Large nonlinear optical coefficients in pseudo-tetragonal BiFeO<sub>3</sub> thin films

Ryan C. Haislmaier, Nikolas J. Podraza, Sava Denev, Alex Melville, Darrell G. Schlom, and Venkatraman Gopalan

Citation: *Applied Physics Letters* **103**, 031906 (2013); doi: 10.1063/1.4812978

View online: <http://dx.doi.org/10.1063/1.4812978>

View Table of Contents: <http://scitation.aip.org/content/aip/journal/apl/103/3?ver=pdfcov>

Published by the AIP Publishing

---

### Articles you may be interested in

[Nonlinear optical and magnetic properties of BiFeO<sub>3</sub> harmonic nanoparticles](#)

*J. Appl. Phys.* **116**, 114306 (2014); 10.1063/1.4895836

[Optimization of excess Bi doping to enhance ferroic orders of spin casted BiFeO<sub>3</sub> thin film](#)

*J. Appl. Phys.* **115**, 234105 (2014); 10.1063/1.4884680

[The conduction mechanism of large on/off ferroelectric diode currents in epitaxial \(111\) BiFeO<sub>3</sub> thin film](#)

*J. Appl. Phys.* **113**, 184106 (2013); 10.1063/1.4804144

[Effect of \(Bi, La\)\(Fe, Zn\)O<sub>3</sub> thickness on the microstructure and multiferroic properties of BiFeO<sub>3</sub> thin films](#)

*J. Appl. Phys.* **112**, 094109 (2012); 10.1063/1.4764340

[Linear and nonlinear optical properties of Bi Fe O 3](#)

*Appl. Phys. Lett.* **92**, 121915 (2008); 10.1063/1.2901168

---

An advertisement for Oxford Instruments' Asylum Research AFM. The background is a dark blue gradient. On the left, there is a black mobile phone and a white desktop computer. Text reads: 'You don't still use this cell phone' and 'or this computer'. In the center, there is a white AFM instrument. Text reads: 'Why are you still using an AFM designed in the 80's?'. On the right, there is more text: 'It is time to upgrade your AFM', 'Minimum \$20,000 trade-in discount for purchases before August 31st', and 'Asylum Research is today's technology leader in AFM'. At the bottom right, there is the Oxford Instruments logo and the tagline 'The Business of Science®'. The email address 'dropmyoldAFM@oxinst.com' is also present.

# Large nonlinear optical coefficients in pseudo-tetragonal BiFeO<sub>3</sub> thin films

Ryan C. Haislmaier,<sup>1,a)</sup> Nikolas J. Podraza,<sup>2</sup> Sava Denev,<sup>1</sup> Alex Melville,<sup>3</sup>  
 Darrell G. Schlom,<sup>3,4</sup> and Venkatraman Gopalan<sup>1,b)</sup>

<sup>1</sup>Department of Materials Science and Engineering, Penn State University, University Park, Pennsylvania 16802, USA

<sup>2</sup>Department of Physics and Astronomy, University of Toledo, Toledo, Ohio 43606, USA

<sup>3</sup>Department of Materials Science and Engineering, Cornell University, Ithaca, New York 14853, USA

<sup>4</sup>Kavli Institute at Cornell for Nanoscale Science, Ithaca, New York 14853, USA

(Received 16 April 2013; accepted 14 June 2013; published online 16 July 2013)

Biaxial strain induces a phase transition from a pseudo-rhombohedral (R) to pseudo-tetragonal (T) phase in BiFeO<sub>3</sub> (BFO) thin films. Using optical second harmonic generation, we measure the nonlinear optical  $d_{ij}$  coefficients at a fundamental wavelength of 1550 nm for R and T-BFO thin films. A large increase of the  $d_{ij}$  magnitudes is observed for T-BFO in comparison to R-BFO. The  $d_{ij}$  magnitudes for T-BFO were measured to be:  $|d_{33}| = 18.1 \pm 2.4$ ,  $|d_{31}| = 60.8 \pm 8.1$ , and  $|d_{15}| = 47.0 \pm 4.2$ , and for R-BFO:  $|d_{33}| = 15.1 \pm 2.1$ ,  $|d_{31}| = 8.5 \pm 1.2$ ,  $|d_{15}| = 0.9 \pm 0.1$ , and  $|d_{22}| = 18.7 \pm 2.6$  (pm/V). The strain-enhanced nonlinear optical properties of T-BFO thin films make them potentially useful for optical applications. © 2013 AIP Publishing LLC.  
[\[http://dx.doi.org/10.1063/1.4812978\]](http://dx.doi.org/10.1063/1.4812978)

BiFeO<sub>3</sub> (BFO) is one of the most intensely studied multi-ferroic materials due to the coexistence of a strong ferroelectric polarization ( $P_s \sim 90 \mu\text{C}/\text{cm}^2$ ) and weak ferromagnetism ( $\sim 0.02 \mu_B/\text{unit cell}$ ) at room temperature.<sup>1–3</sup> Recently, BFO has also been recognized as a promising candidate for many photonic applications ranging from terahertz wave generation,<sup>4,5</sup> electro-optical modulation,<sup>6</sup> infrared detection,<sup>7</sup> photoconduction,<sup>8,9</sup> and ultrafast devices.<sup>10</sup> It has been shown that a structural phase transition from a pseudo-rhombohedral (R) to pseudo-tetragonal (T) phase occurs at  $\sim -4.5\%$  compressive strain,<sup>11–14</sup> where increased ferroelectric polarization and electromechanical responses have been reported.<sup>15,16</sup> Using optical second harmonic generation (SHG) analysis, we observe enhanced nonlinear optical (NLO) properties in T-BFO thin films. As future photonic applications for BFO thin films are realized, the investigation of strain-enhanced nonlinear optical properties could play a vital role for optimizing material performance and functionality.

In previous works, the nonlinear optical  $d_{ij}$  coefficients of R-BFO have been reported, although there are discrepancies in the literature. Using density functional theory, Ju *et al.* calculated the spectroscopic  $d_{ij}$  values for bulk BFO<sup>17</sup> and strained T-BFO<sup>18</sup> systems, which we will henceforth refer to as *theory*. Kumar *et al.*<sup>19</sup> reported  $d_{ij}$  values of a R-BFO thin film at a fundamental wavelength of 800 nm that are not consistent with theory, which can be attributed to an incorrect SHG model (Eq. (4) in Ref. 19). Yokota *et al.*<sup>20</sup> measured the  $d_{ij}$  coefficient ratios for bulk BFO at 1064 nm, however, their reported values are also inconsistent with theory. There are no reports on the measured  $d_{ij}$  coefficient values for T-BFO thin films. In order to address these discrepancies in the literature, we formulate a method to accurately measure the coefficients for a thin film/substrate system, and we report  $d_{ij}$  coefficient values at 1550 nm for both R and T-BFO films which are consistent with theory.

The films studied here were grown by reactive molecular-beam epitaxy,<sup>11</sup> with well defined orientations of R and T-BFO on (111) SrTiO<sub>3</sub> (STO) and (110) YAlO<sub>3</sub> (YAO) substrates with lattice misfit strains of  $-1.1\%$  and  $-6.9\%$ , respectively. The orientation of the 25 nm thick R-BFO film is  $(111)_p\text{BFO} \parallel (111)\text{STO}$  and  $[1\bar{1}0]_p\text{BFO} \parallel [1\bar{1}0]\text{STO}$ , with the crystal physics axes defined as:  $z_1 = [110]_p$ ,  $z_2 = [11\bar{2}]_p$ , and  $z_3 = [111]_p$ , where subscript p denotes the pseudo-cubic indices. The orientation of the 25 nm thick T-BFO film is  $(001)\text{BFO} \parallel (110)\text{YAO}$  and  $[010]\text{BFO} \parallel [1\bar{1}0]\text{YAO}$ , with the crystal physics axes defined as:  $z_1 = [100]$ ,  $z_2 = [010]$ , and  $z_3 = [001]$ . X-ray diffraction measurements, shown in Fig. S.1 of the supplementary material,<sup>21</sup> yield a lattice parameter of  $a_p = 3.958 \pm 0.002 \text{ \AA}$  for R-BFO, and lattice parameters  $c = 4.670 \pm 0.001 \text{ \AA}$  and  $a = 3.751 \pm 0.002 \text{ \AA}$  for T-BFO. We ignore the small monoclinic distortions of the films and treat them as pure tetragonal ( $4mm$  point group symmetry) and rhombohedral ( $3m$  point group symmetry) phases for our analysis, which we show later to be justified. Piezoresponse force microscopy measurements indicate that the films are single-domain, which is consistent with other reports.<sup>11,22,23</sup>

Optical SHG is a process where light at frequency  $\omega$  (electric field  $E_\omega$ ) is converted into light at frequency  $2\omega$  by a nonlinear material, through the creation of a nonlinear polarization,  $P_{i,2\omega} \propto d_{ijk}E_{j,\omega}E_{k,\omega}$ , where  $d_{ijk}$  is the nonlinear optical coefficient tensor, which can be expressed as  $d_{ij}$  in Voigt notation.<sup>24</sup> To accurately measure the  $d_{ij}$  coefficient values of a nonlinear material, the refractive index ( $n$ ) and extinction coefficient ( $k$ ) at the fundamental and SHG wavelengths must be precisely known. Spectroscopic ellipsometry measurements were performed to determine these values. The onset of absorption for the R and T-BFO films occurs at approximately 577 nm and 588 nm, respectively, which are near other values reported for BFO thin films.<sup>19,26</sup> Absorption adds additional complications to the SHG modeling, therefore, we chose a fundamental wavelength of 1550 nm (frequency  $\omega$ ) where the corresponding SHG wavelength at 775 nm (frequency  $2\omega$ ) is far from resonance for both films ( $k < 10^{-2}$ ).

<sup>a)</sup>Electronic mail: RyanHaislmaier@gmail.com

<sup>b)</sup>Electronic mail: vxg8@psu.edu

The refractive indices for the R and T-BFO films at  $\omega$  ( $2\omega$ ) are  $n_{\omega}^R = 2.72$  ( $n_{2\omega}^R = 2.85$ ) and  $n_{\omega}^T = 2.54$  ( $n_{2\omega}^T = 2.63$ ), respectively. The Mueller matrix spectra collected for both films indicate relatively weak optical anisotropy and are treated as being optically isotropic in our analysis.

SHG experiments were performed using a 1550 nm fundamental laser beam (120 fs pulse width, 1 kHz repetition rate) which was generated from a Spectra-Physics Ti:sapphire pumped OPA-800C. The fundamental beam power used for these experiments was approximately  $1.5 \text{ W/cm}^2$  for a beam waist diameter of  $50 \mu\text{m}$ . No SHG signal was detected from the STO or YAO substrates at this incident power. The experimental geometry is shown in Fig. 1, where the linearly polarized fundamental electric field,  $E_{\omega}$ , is rotated by an angle  $\phi$  and incident to the film normal at an angle  $\theta$  in the  $x$ - $z$  plane. The  $p$ -polarized ( $\parallel$ ) transmitted SHG field is denoted as  $E_{2\omega\parallel}$ . Note that  $p$ -polarized refers to the component of the electric field which is parallel to the plane of incidence ( $x$ - $z$  plane) and the  $s$ -polarized component is perpendicular to the plane of incidence ( $y$ -axis). We employ two experimental configurations for our SHG characterization: (1) *tilt-scans*, where  $\phi$  is fixed and the sample is rotated by  $\pm\theta$ , and (2) *polar-plots*, where  $\theta$  is fixed and  $\phi$  is rotated by  $360^\circ$ . The R-BFO film has two unique sample tilt axes due to the anisotropy between the  $z_1$  and  $z_2$  crystal physics axes for  $3m$  point group symmetry, where we define the two unique sample tilt configurations as (1)  $z_1 = y, z_2 = -x, z_3 = z$ , henceforth abbreviated as  $R_1$ , and (2)  $z_1 = -y, z_2 = x, z_3 = z$ , abbreviated as  $R_2$ . The T-BFO film has only one unique sample tilt axis since  $z_1$  and  $z_2$  are symmetrically equivalent in  $4mm$  point group symmetry, and we define the sample tilt configuration as  $z_1 = x, z_2 = y, z_3 = z$ , abbreviated as  $T_1$ .

First, we determine the  $d_{ij}$  coefficient ratios ( $K_{ij} = d_{ij}/d_{15}$ ) of the BFO films through transmission SHG polarimetry analysis. A series of tilt scans and polar plots were collected in the configurations described above for the R and T-BFO films, shown in Figs. 2 and 3, respectively. Theoretical fitting of the SHG data was performed using an analytical model for the  $p$ -polarized transmitted SHG intensity for an isotropic nonlinear thin film (denoted as superscript  $f$ ) on a substrate, which is defined as<sup>27</sup>

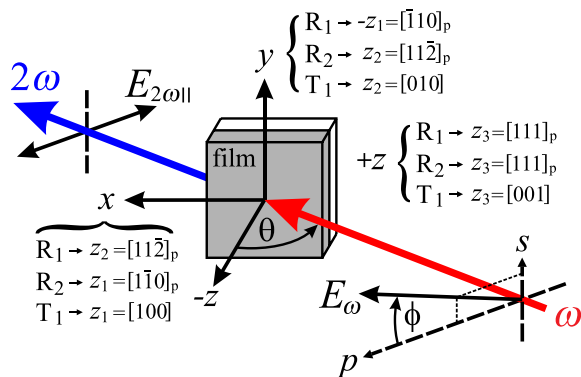


FIG. 1. SHG polarimetry geometry showing the linearly polarized fundamental field,  $E_{\omega}$ , rotated by an angle  $\phi$  and incident to the film normal by an angle  $\theta$  in the  $x$ - $z$  plane, and the  $p$ -polarized ( $\parallel$ ) SHG field,  $E_{2\omega\parallel}$ . Also shown are the orientations of the film crystal physics axes ( $z_1, z_2, z_3$ ) for the  $R_1$  ( $z_1 = y, z_2 = -x, z_3 = z$ ),  $R_2$  ( $z_1 = -y, z_2 = x, z_3 = z$ ), and  $T_1$  ( $z_1 = x, z_2 = y, z_3 = z$ ) configurations.

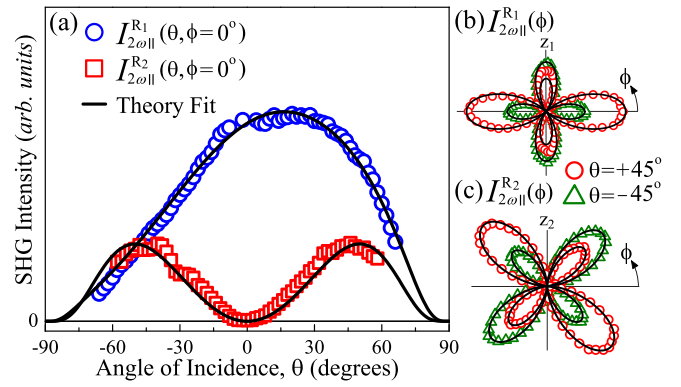


FIG. 2. SHG polarimetry data of R-BFO at 1550 nm showing the transmitted  $p$ -polarized SHG intensity in the  $R_1$  and  $R_2$  configurations for the (a) tilt scans,  $I_{2\omega\parallel}^{R_1}(\theta, \phi = 0^\circ)$  (blue circles),  $I_{2\omega\parallel}^{R_2}(\theta, \phi = 0^\circ)$  (red squares), where  $I_{2\omega\parallel}^{R_2}$  is scaled by a factor of  $5\times$  for comparison, and polar plots, (b)  $I_{2\omega\parallel}^{R_1}(\phi)$  and (c)  $I_{2\omega\parallel}^{R_2}(\phi)$  at  $\theta = +45^\circ$  (red circles) and  $\theta = -45^\circ$  (green triangles). Theoretical fits are shown as black lines.

$$I_{2\omega\parallel}^f = (I_{\omega})^2 (2\pi L/\lambda_{\omega})^2 (d_{\text{eff}}^f)^2 \Theta_f, \quad (1)$$

where  $L$  is the film thickness,  $\lambda_{\omega}$  and  $I_{\omega}$  are the wavelength and intensity of the fundamental laser beam, respectively, and  $\Theta_f$  accounts for the transmittance and reflectance of the fundamental and SHG fields in the film, which is explicitly defined in the supplementary material.<sup>21</sup> The  $d_{\text{eff}}^f$  term is the effective  $d$  coefficient, which is dependent on the form of the  $d_{ijk}$  tensor and the orientation of the fundamental electric field with respect to the crystal physics axes of the film, and is defined as  $d_{\text{eff}}^f = \hat{e}_{2\omega\parallel} \cdot d'_{ijk} \hat{e}_{j,\omega} \hat{e}_{k,\omega}$ . Here,  $d'_{ijk}$  is the transformed  $d_{ijk}$  tensor in the  $x, y, z$  coordinate system, and the polarization unit vectors are given by  $\hat{e}_{2\omega\parallel} = (\cos\theta_{2\omega}, 0, -\sin\theta_{2\omega})$ , and  $\hat{e}_{\omega} = (t_{\omega\parallel}^{\text{af}} \cos\phi \cos\theta_{\omega}, t_{\omega\perp}^{\text{af}} \sin\phi, -t_{\omega\parallel}^{\text{af}} \cos\phi \sin\theta_{\omega})$ . The transmission ( $t$ ) fresnel coefficients for  $p$ -polarized and  $s$ -polarized ( $\perp$ ) light at the air/film (af) interface are defined as  $t_{\omega\parallel}^{\text{af}} = 2\cos\theta/(\cos\theta_{\omega} + n_{\omega}\cos\theta)$ , and  $t_{\omega\perp}^{\text{af}} = 2\cos\theta/(n_{\omega}\cos\theta_{\omega} + \cos\theta)$ , where  $\theta_{\omega}$  ( $\theta_{2\omega}$ ) are the refracted angles of the fundamental (SHG) inside of the film. We define irreducible expressions of  $d_{\text{eff}}^f$  as a function of the  $K_{ij}$  parameters for the  $R_1, R_2$ , and  $T_1$  film configurations, where we use the notation  $f \rightarrow (R_1, R_2, T_1)$ , which are given by

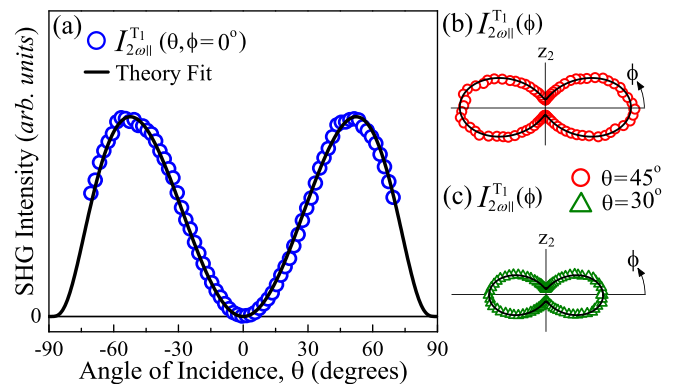


FIG. 3. SHG polarimetry data of T-BFO at 1550 nm, showing the transmitted  $p$ -polarized SHG intensity in the  $T_1$  configuration for the (a) tilt scan,  $I_{2\omega\parallel}^{T_1}(\theta, \phi = 0^\circ)$  (blue circles), and polar plots, (b)  $I_{2\omega\parallel}^{T_1}(\phi, \theta = 45^\circ)$  (red circles), and (c)  $I_{2\omega\parallel}^{T_1}(\phi, \theta = 30^\circ)$  (green triangles). Theoretical fits are shown as black lines.

$$\begin{aligned}
d_{\text{eff}}^{\text{R}_1}/d_{15} &= \cos \theta_{2\omega} \{ [t_{\omega\parallel}^{\text{af}}]^2 (K_{22} \cos^2 \theta_{\omega} - \sin 2\theta_{\omega}) \cos^2 \phi - [t_{\omega\perp}^{\text{af}}]^2 K_{22} \sin^2 \phi \} \\
&\quad - \sin \theta_{2\omega} \{ [t_{\omega\parallel}^{\text{af}}]^2 (K_{31} \cos^2 \theta_{\omega} + K_{33} \sin^2 \theta_{\omega}) \cos^2 \phi + [t_{\omega\perp}^{\text{af}}]^2 K_{31} \sin^2 \phi \}, \\
d_{\text{eff}}^{\text{R}_2}/d_{15} &= -\cos \theta_{2\omega} \{ [t_{\omega\parallel}^{\text{af}}]^2 \sin 2\theta_{\omega} \cos^2 \phi + [t_{\omega\parallel}^{\text{af}}][t_{\omega\perp}^{\text{af}}] K_{22} \cos \theta_{\omega} \sin^2 \phi \} \\
&\quad - \sin \theta_{2\omega} \{ [t_{\omega\parallel}^{\text{af}}]^2 (K_{31} \cos^2 \theta_{\omega} + K_{33} \sin^2 \theta_{\omega}) \cos^2 \phi + [t_{\omega\perp}^{\text{af}}]^2 K_{31} \sin^2 \phi \}, \\
d_{\text{eff}}^{\text{T}_1}/d_{15} &= -\cos \theta_{2\omega} \{ [t_{\omega\parallel}^{\text{af}}]^2 \sin 2\theta_{\omega} \cos^2 \phi \} - \sin \theta_{2\omega} \{ [t_{\omega\parallel}^{\text{af}}]^2 (K_{31} \cos^2 \theta_{\omega} + K_{33} \sin^2 \theta_{\omega}) \cos^2 \phi + [t_{\omega\perp}^{\text{af}}]^2 K_{31} \sin^2 \phi \}.
\end{aligned} \tag{2}$$

The  $K_{ij}$  parameters were extracted from theoretical fits according to Eq. (1) to the SHG polarimetry data. The fits yield the following  $K_{ij}$  values for R-BFO:  $K_{33} = 17.3 \pm 1.7$ ,  $K_{31} = 9.7 \pm 1.0$ , and  $K_{22} = -21.4 \pm 2.1$  and for T-BFO:  $K_{33} = -0.4 \pm 0.04$  and  $K_{31} = 1.3 \pm 0.1$ . We note that other  $K_{ij}$  parameter solution sets exist which yield satisfactory fits to experimental data; having estimates of the NLO coefficient values via theoretical calculations *a priori* is helpful in identifying the correct parameter solution set.

As seen from Eqs. (1) and (2), for a  $p$ -polarized incident field ( $\phi = 0^\circ$ ),  $I_{2\omega\parallel}^{\text{R}_2}$  and  $I_{2\omega\parallel}^{\text{T}_1}$  go to zero at normal incidence ( $\theta = 0^\circ$ ), and should also be symmetric about  $\theta = 0^\circ$ , which is clearly observed in the tilt scans shown in Fig. 2(a) (red squares) and Fig. 3(a) (blue circles) for the R and T-BFO films, respectively. Any significant monoclinicity in the films would result in non-zero SHG intensities at normal incidence and asymmetric tilt scans.<sup>25</sup> This indicates that the films studied here behave like pure rhombohedral and tetragonal phases.

Next, we measure the absolute magnitude of the reflected effective  $d$  coefficient,  $d_{\text{eff}}^{r,f}$ , of the films with respect to a congruently grown  $z$ -cut LiNbO<sub>3</sub> (LNO) reference crystal with well known linear and nonlinear optical properties.<sup>28</sup> This measurement is made in reflection geometry since we can avoid having to precisely know the thickness of the reference crystal, where small errors in the reference thickness can result in large errors of the measured  $d_{ij}$  values of the film.<sup>27</sup> By wedging and roughening the backside interface of the reference crystal, the collinear back reflections from that interface are diverted and scattered, where only the SHG reflected from the incident interface is allowed to propagate, and the thickness parameter does not need to be considered. Following the boundary-condition approach outlined in Ref. 27, we derive expressions for the  $p$ -polarized reflected SHG intensity for an isotropic nonlinear thin film/substrate system and the  $p$ -polarized reflected SHG intensity from a single interface of a birefringent nonlinear reference (denoted as superscript ref), which are defined as

$$\begin{aligned}
I_{2\omega\parallel}^{r,f} &= (I_{\omega}^f)^2 (2\pi L/\lambda_{\omega})^2 (d_{\text{eff}}^{r,f})^2 \Pi_f, \\
I_{2\omega\parallel}^{r,\text{ref}} &= (I_{\omega}^{\text{ref}})^2 (d_{\text{eff}}^{r,\text{ref}})^2 \Omega_{\text{ref}},
\end{aligned} \tag{3}$$

where  $\Pi_f$  and  $\Omega_{\text{ref}}$  account for the reflectance and transmittance of the fundamental and SHG fields in the film and reference, respectively (complete definitions are provided in the supplementary material<sup>21</sup>) and  $d_{\text{eff}}^{r,\text{ref}}$  is the reflected effective  $d$  coefficient of the reference. The  $z$ -cut LNO reference crystal has the same point group symmetry ( $3m$ ) and crystal physics axes orientation as R-BFO, so the same configurations

( $\text{R}_1, \text{R}_2$ ) apply. In the reflected geometry,  $d_{\text{eff}}^{r,f} = \hat{\mathbf{e}}_{2\omega\parallel}^r \cdot d'_{ijk} \hat{\mathbf{e}}_{j,\omega} \hat{\mathbf{e}}_{k,\omega}$ , where  $\hat{\mathbf{e}}_{2\omega\parallel}^r = (-\cos \theta_{2\omega}, 0, -\sin \theta_{2\omega})$ . Therefore,  $d_{\text{eff}}^{r,f}$  is identical to the expressions in Eq. (2) except that the sign in front of the  $\cos \theta_{2\omega}$  term is reversed. Taking the ratio of the two expressions in Eq. (3), we can solve for  $d_{\text{eff}}^{r,f}$  as

$$|d_{\text{eff}}^{r,f}| = |d_{\text{eff}}^{r,\text{ref}}(\lambda_{\omega}/2\pi L)(I_{\omega}^{\text{ref}}/I_{\omega}^f)(I_{2\omega\parallel}^{r,f}/I_{2\omega\parallel}^{r,\text{ref}}\Pi_f)^{1/2}|. \tag{4}$$

We measured the values of  $I_{2\omega}^{\text{R}_1}$ ,  $I_{2\omega}^{\text{T}_1}$ , and  $I_{2\omega}^{\text{LNO}(\text{R}_1)}$  at  $\theta = 45^\circ$  and  $\phi = 0^\circ$ , where the fundamental intensity at the film and reference interfaces was kept constant between subsequent measurements ( $I_{\omega\parallel}^f = I_{\omega\parallel}^{\text{ref}}$ ) by mounting the samples with their incident interfaces lying in the same plane, and by translating the samples parallel to the rotation axis. Then, by substituting these measured intensity values and the known linear optical properties of the films and reference into Eq. (4) (at  $\theta = 45^\circ$ ,  $\phi = 0^\circ$ ), we find that for R-BFO,  $|d_{\text{eff}}^{r,\text{R}_1}| = 3.6 \pm 0.3$  pm/V, and for T-BFO,  $|d_{\text{eff}}^{r,\text{T}_1}| = 2.6 \pm 0.2$  pm/V. With subsequent use of Eq. (2) and the already determined  $K_{ij}$  values, we calculate  $|d_{15}| = 0.9 \pm 0.1$  pm/V for R-BFO and  $|d_{15}| = 47.0 \pm 4.2$  pm/V for T-BFO, where the absolute magnitudes of the other  $d_{ij}$  coefficients can be directly calculated from the  $K_{ij}$  parameters. Note that only the absolute magnitudes of the  $d_{ij}$  coefficients can be determined using this technique; only the signs of the  $d_{ij}$  coefficient ratios ( $K_{ij}$ ) can be unambiguously resolved. According to the theoretical calculations by Ju *et al.*,  $d_{15} = -1.0$  pm/V for bulk BFO<sup>17</sup> and  $d_{15} = 53.0$  pm/V for T-BFO.<sup>18</sup> Using the  $d_{15}$  sign conventions from theory, we have listed in Table I the measured  $d_{ij}$  coefficients for R and T-BFO from this work along with the theoretical values<sup>29</sup> for comparison, which are in very good agreement.

For the T-BFO film, we observe a large increase of the  $d_{ij}$  magnitudes with respect to R-BFO, where the largest T-BFO

TABLE I. Nonlinear optical  $d_{ij}$  (pm/V) coefficient values from this work and theoretical values reported by Ju *et al.* for R and T-BFO thin films at 1550 nm.

$d_{ij}$	Rhombohedral $3m$		Tetragonal $4mm$	
	This work	Theory <sup>a</sup>	This work	Theory <sup>b</sup>
$d_{33}$	$-15.1 \pm 2.1$	-19.1	$-18.1 \pm 2.4$	-18.6
$d_{31}$	$-8.5 \pm 1.2$	-10.7	$60.8 \pm 8.1$	66.1
$d_{15}$	$-0.9 \pm 0.1$	-1.0	$47.0 \pm 4.2$	53.0
$d_{22}$	$18.7 \pm 2.6$	21.4	...	...

<sup>a</sup>Reference 17.

<sup>b</sup>Reference 18.

coefficient ( $|d_{31}| = 60.8 \pm 8.1$  pm/V) is approximately 325% greater than the largest R-BFO coefficient ( $|d_{22}| = 18.7 \pm 2.6$  pm/V). The large  $d_{ij}$  magnitudes of both R and T-BFO films rival standard nonlinear optical materials such as LiNbO<sub>3</sub> ( $|d_{33}| = 27.2$  pm/V at 1064 nm), KNbO<sub>3</sub> ( $|d_{33}| = 19.6$  pm/V at 1064 nm), and BaTiO<sub>3</sub> ( $|d_{31}| = 14.4$  pm/V at 1064 nm).<sup>28</sup> The strain-enhanced  $d_{ij}$  magnitudes in T-BFO films found here are consistent with other reported property enhancements such as an increased polarization and strong electromechanical responses,<sup>11,15</sup> which is believed to arise from the strain-induced super-tetragonality in the T-BFO system.<sup>12,16</sup>

In summary, we report the measured nonlinear optical  $d_{ij}$  coefficients at 1550 nm for R and T-BFO thin films which are consistent with theory, and we have also outlined a general experimental method to measure these values for a thin film/substrate system. We observe a large increase in the  $d_{ij}$  coefficient magnitudes for the T-BFO film in comparison to R-BFO, where both the R and T-BFO films strongly challenge the standard nonlinear optical materials currently used today. The large  $d_{ij}$  magnitudes and low optical absorption in T-BFO films make them potentially useful for optical applications and device integration, where the ability to strain-tune thin films provides an encouraging route for enhancing the nonlinear optical performance of materials.

The authors acknowledge financial support from the National Science Foundation through the MRSEC program Grant Nos. DMR-1210588, DMR-0908718, and DMR-0820404. The work at Cornell University was supported by ARO through Agreement No. W911NF-08-2-0032.

<sup>1</sup>J. Wang, J. B. Neaton, H. Zheng, V. Nagarajan, S. B. Ogale, B. Liu, D. Viehland, V. Vaithyanathan, D. G. Schlom, U. V. Waghmare, N. A. Spaldin, K. M. Rabe, M. Wuttig, and R. Ramesh, *Science* **299**, 1719 (2003).

<sup>2</sup>C. Ederer and N. Spaldin, *Phys. Rev. B* **71**, 224103 (2005).

<sup>3</sup>G. Catalan and J. F. Scott, *Adv. Mater.* **21**, 2463 (2009).

<sup>4</sup>K. Takahashi, N. Kida, and M. Tonouchi, *Phys. Rev. Lett.* **96**, 117402 (2006).

<sup>5</sup>D. Talbayev, S. Lee, S.-W. Cheong, and A. J. Taylor, *Appl. Phys. Lett.* **93**, 212906 (2008).

<sup>6</sup>J. Allibe, K. Bougot-Robin, E. Jacquet, I. C. Infante, S. Fusil, C. Carretero, J.-L. Reverchon, B. Marchihac, D. Crete, J.-C. Mage, A. Barthelemy, and M. Bibes, *Appl. Phys. Lett.* **96**, 182902 (2010).

<sup>7</sup>Y. Li, J. Xue, J. Sun, X. Meng, Z. Huang, J. Chu, L. Ding, and W. Zhang, *Appl. Phys. A* **87**, 125 (2007).

<sup>8</sup>S. R. Basu, L. W. Martin, Y. H. Chu, M. Gajek, R. Ramesh, R. C. Rai, X. Xu, and J. L. Musfeldt, *Appl. Phys. Lett.* **92**, 091905 (2008).

<sup>9</sup>R. K. Katiyar, A. Kumar, G. Morell, J. F. Scott, and R. S. Katiyar, *Appl. Phys. Lett.* **99**, 092906 (2011).

<sup>10</sup>Z. Jin, Y. Xu, Z. Zhang, G. Li, X. Lin, G. Ma, Z. Cheng, and X. Wang, *Appl. Phys. Lett.* **100**, 071105 (2012).

<sup>11</sup>R. J. Zeches, M. D. Rossell, J. X. Zhang, A. J. Hatt, Q. He, C.-H. Yang, A. Kumar, C. H. Wang, A. Melville, C. Adamo, G. Sheng, Y.-H. Chu, J. F. Ihlefeld, R. Erni, C. Ederer, V. Gopalan, L. Q. Chen, D. G. Schlom, N. A. Spaldin, L. W. Martin, and R. Ramesh, *Science* **326**, 977 (2009).

<sup>12</sup>H. Bea, B. Dupe, S. Fusil, R. Mattana, E. Jacquet, B. Warot-Fonrose, F. Wilhelm, A. Rogalev, S. Petit, V. Cros, A. Anane, F. Petroff, K. Bouzehouane, G. Geneste, B. Dkhil, S. Lisenkov, I. Ponomareva, L. Bellaiche, M. Bibes, and A. Barthelemy, *Phys. Rev. Lett.* **102**, 217603 (2009).

<sup>13</sup>A. J. Hatt and N. A. Spaldin, *Phys. Rev. B* **81**, 054109 (2010).

<sup>14</sup>H. Christe, J. Nam, H. Kim, A. Hatt, and N. Spaldin, *Phys. Rev. B* **83**, 144107 (2011).

<sup>15</sup>K. Y. Yun, D. Ricinchi, Y. Kanashima, M. Noda, and M. Okuyama, *Jpn. J. Appl. Phys., Part 2* **43**, L647 (2004).

<sup>16</sup>D. Ricinchi, K.-Y. Yun, and M. Okuyama, *J. Phys.: Condens. Matter* **18**, L97 (2006).

<sup>17</sup>S. Ju, T.-Y. Cai, and G.-Y. Guo, *J. Chem. Phys.* **130**, 214708 (2009).

<sup>18</sup>S. Ju and T.-Y. Cai, *Appl. Phys. Lett.* **95**, 112506 (2009).

<sup>19</sup>A. Kumar, R. C. Rai, N. J. Podraza, S. Denev, M. Ramirez, Y.-H. Chu, L. W. Martin, J. Ihlefeld, T. Heeg, J. Schubert, D. G. Schlom, J. Orenstein, R. Ramesh, R. W. Collins, J. L. Musfeldt, and V. Gopalan, *Appl. Phys. Lett.* **92**, 121915 (2008).

<sup>20</sup>H. Yokota, R. Haumont, J.-M. Kiat, H. Matsuura, and Y. Uesu, *Appl. Phys. Lett.* **95**, 082904 (2009).

<sup>21</sup>See supplementary material at <http://dx.doi.org/10.1063/1.4812978> for x-ray diffraction data and complete definitions of the terms  $\Theta_f$ ,  $\Pi_f$ , and  $\Omega_{ref}$ .

<sup>22</sup>Y. C. Chen, Q. R. Lin, and Y. H. Chu, *Appl. Phys. Lett.* **94**, 122908 (2009).

<sup>23</sup>Y.-H. Chu, M. Cruz, C.-H. Yang, L. Martin, P.-L. Yang, J.-X. Zhang, K. Lee, P. Yu, L.-Q. Chen, and R. Ramesh, *Adv. Mater.* **19**, 2662 (2007).

<sup>24</sup>S. A. Denev, T. A. Ludden, E. Barnes, A. Kumar, and V. Gopalan, *J. Am. Ceram. Soc.* **94**(9), 2699 (2011).

<sup>25</sup>A. Kumar, S. Denev, R. J. Zeches, E. Vlahos, N. J. Podraza, A. Melville, D. G. Schlom, R. Ramesh and V. Gopalan, *Appl. Phys. Lett.* **97**, 112903 (2010).

<sup>26</sup>P. Chen, N. J. Podraza, X. S. Xu, A. Melville, E. Vlahos, V. Gopalan, R. Ramesh, D. G. Schlom, and J. L. Musfeldt, *Appl. Phys. Lett.* **96**, 131907 (2010).

<sup>27</sup>W. N. Herman and L. M. Hayden, *J. Opt. Soc. Am. B* **12**, 416 (1995).

<sup>28</sup>D. N. Nikogosyan, *Nonlinear Optical Crystals: A Complete Survey* (Springer, New York, 2005), pp. 35–64.

<sup>29</sup>Theoretical  $d_{ij}$  values listed in Table I were taken from Fig. 7 from Ref. 17 for bulk BFO and from Fig. 2 from Ref. 18 for T-BFO.